JOURNAL OF AIRCRAFT
Vol. 30, No. 6, Nov.–Dec. 1993

Investigation of Rotor Tip Vortex Interactions with a Body

Nai-Pei Bi,* J. Gordon Leishman,† and Gilbert L. Crouse Jr.‡
University of Maryland, College Park, College Park, Maryland 20742

Experiments were conducted to examine rotor tip vortex interactions with a body in low-speed forward flight. Unsteady pressure measurements were made at points along the top and around the circumference of the body surface. Flow visualization of the rotor wake was performed using the wide-field shadowgraph method. Considerable insight into the tip vortex interaction processes was obtained by correlating the pressure loads with the vortex trajectories as they approached, distorted, and impinged on the body surface. Unsteady potential flow theory was explored as a means of predicting the unsteady pressure loads on the body surface, using prescribed tip vortex trajectories measured from flow visualization. The results have shown that the process of tip vortex interaction with a body can be divided into three regimes: 1) close tip vortex/body interactions, which is an inviscid flow regime; 2) vortex/surface impingement; and 3) postvortex/surface impingement; the latter involves viscous effects. The results have also shown that the pressures at points on the body exhibited a high sensitivity to tip vortex convection speed and location, which makes the general prediction of such interactional phenomena difficult with existing rotor/airframe interaction models.

Nomenclature

C_T = rotor thrust coefficient, $T/(\rho\pi\Omega^2R^4)$
C^u_{Fy} = body sectional side force coefficient, $-\int_0^{2\pi} C^u_p(\phi)\sin\phi\, d\phi$
C^u_{Fz} = body sectional normal force coefficient, $-\int_0^{2\pi} C^u_p(\phi)\cos\Phi\, d\Phi$
C^u_p = unsteady pressure coefficient, $100(p^u - p_\infty)/(\frac{1}{2}\rho\Omega^2R^2)$
c = blade chord, m
N_b = number of blades
p^u = unsteady component of pressure, Pa
p_∞ = static pressure, Pa
R = rotor radius, m
T = rotor thrust, N
t = time, s
V_i = velocity induced at a point by vortex, m/s
V_{vor} = convection velocity of vortex, m/s
V_x = x component of vortex convection velocity, m/s
V_z = z component of vortex convection velocity, m/s
V_∞ = freestream velocity, m/s
v = local flow velocity, m/s
α_{TPP} = tip-path plane angle of attack, deg
Γ = vortex strength, m²/s
λ = rotor inflow ratio
μ = advance ratio, $V_\infty/\omega R$
ρ = air density, kg/m³
σ = rotor solidity, $N_bc/\pi R$
Φ = body circumferential angle, deg
ϕ = velocity potential
χ = wake skew angle, deg
ψ = blade azimuth angle, deg
ψ_w = tip vortex (wake) age, deg
Ω = rotational frequency, rad/s

Received Sept. 5, 1991; presented as Paper 91-3228 at the AIAA 9th Applied Aerodynamics Conference, Baltimore, MD, Sept. 23–26, 1991; revision received June 29, 1992; accepted for publication Aug. 20, 1992.

*Research Associate, Center for Rotorcraft Education and Research, Department of Aerospace Engineering; currently Engineering Specialist, Advanced Technologies, Inc., Newport News, Virginia.

†Assistant Professor, Center for Rotorcraft Education and Research, Department of Aerospace Engineering. Member AIAA.

‡Graduate Fellow, Center for Rotorcraft Education and Research, Department of Aerospace Engineering.

Introduction

HELICOPTER rotors produce energetic vortical wakes which can strongly interact with the airframe. Several investigators, including Bramwell,[1] Sheridan,[2] Komerath et al.,[3] and Bi and Leishman,[4] have shown that the unsteady airloads induced by the rotor and its wake are a dominant form of loading on the airframe. These unsteady loads are induced mainly by the pressure field due to the passing blades and the interaction of discrete rotor tip vortices with the airframe surface. The magnitude of the unsteady loads induced on the airframe are such that they can affect vibration levels and handling qualities.[5]

Rotor wake and tip vortex interactions with the helicopter airframe are a particularly acute problem in hover, and in forward flight at low advance ratios. Under these conditions, the intense rotor tip vortices are convected close to, or may impinge directly on, parts of the airframe. While tip vortex impingement is a localized problem, significant transient loads are produced[2,4] which appear difficult to predict by means of existing analytical methods.[6,7] In addition, the airframe distorts the rotor tip vortex trajectories during this process, resulting in a change in induced inflow through the rotor disk. This will produce a change in rotor performance and blade loads. The significant effect of the body on the rotor performance has been measured experimentally in both hover[8,9] and forward flight,[10] but the effects have not yet been predicted with sufficient accuracy.

The understanding of the flow behavior and loads induced by vortices convected toward solid surfaces is a very complicated problem in fluid dynamics. Interactions of vortices with planar surfaces have been studied by Lim,[11] Atias and Weihs,[12] Doligalski and Walker,[13] and Walker et al.[14] These works have shown that the vortex/surface interaction problem involves a complex balance of vorticity convection, intensification, and diffusion. For helicopters, similar mechanisms are involved as the rotor tip vortices undergo distortions near the airframe.[9,15] Significant self-induced unsteady (nonperiodic) motion of the tip vortex filaments has also been observed under these conditions.[16]

Predicting the consequences of tip vortex interactions with a helicopter airframe is made difficult by the curved and three-dimensional nature of the tip vortices and the complex curvatures of the airframe surface. Crouse et al.,[6] Quackenbush

et al.,[7] and Lober and Egolf[17] have used both two-dimensional and three-dimensional potential flow theories to investigate vortex/surface interactions and wake impingement phenomena on helicopter airframes. Although some encouraging results have been obtained, satisfactory predictions are difficult and further work is still required before robust numerical models are developed. It is clear that predicting the wake behavior near the fuselage surface with any practical model requires the continued guidance of experiments.

Experiments documenting the behavior of helicopter rotor wakes in forward flight are few, and experiments concerned with the specific effects of an airframe are somewhat rare. Komerath et al.[3,18] and Brand et al.[19] have investigated rotor wake impingement on the nose of a cylindrical body. The wake was created by a two-bladed teetering rotor operating at low-tip Mach numbers. Unsteady pressures were measured on the cylinder surface with off-surface velocity measurements and laser sheet flow visualization. While several interesting results have been obtained, the unrealistically close spacing of the rotor and the body produces extremely large interactional effects between the blades and body. Therefore, the effects produced by the tip vortices cannot be isolated from the more dominant effects of blade passage. Also, as shown by Bramwell,[1] and more recently by Crouse and Leishman,[20] when the body is extremely close to the rotor, it strongly affects the induced velocity and circulation on the blades. Because the tip vortex strengths and trajectories are so strongly influenced by these large periodic changes in blade lift, it becomes difficult to decouple the influence of the body on the rotor. The isolation of this effect is desirable for validating theoretical models of the vortex/surface interaction problem.

Recent studies on the rotor/airframe interaction problem have been conducted by Leishman and Bi (see Refs. 4, 10, 21, and 22), using a four-bladed rotor and a body of revolution representing a helicopter fuselage. Measurements were made of the rotor performance, body forces and moments, and body pressure distributions. Flowfield surveys and wake visualization were also conducted.[10] One goal in these experiments was to more completely isolate the effects of different interaction phenomena, i.e., the effects of blade passage from those induced by the tip vortices. These studies have enabled a fuller characterization of the pressure loads induced on the body surface due to different (but related) interactional events, and have provided a more suitable data base for validating theoretical models.[6,23] However, although some progress has been made in the study of rotor wake behavior near and on the body surface, it was clear from the original experiments that the tip vortex/surface impingement process was far from being understood.

This article presents some new results from an investigation of rotor tip vortex interactions with a body. It is shown that considerable insight into the physical features of tip vortex impingement can be gained by correlation studies between the vortex trajectories obtained from flow visualization and the unsteady pressures measured on the body surface.

Description of the Experiment

Experimental Setup

A four-bladed rotor and a body of revolution representing a helicopter fuselage was used for the experiments. Figure 1 shows the general arrangement of the rotor/body system. The rotor was 1.65 m (65 in.) in diameter, and consisted of a fully articulated hub with a conventional swashplate arrangement. Collective and cyclic pitch were remotely controlled using three servo actuators. The blades were rectangular in planform with a 6.35-cm (2.5-in.) chord, and with 13 deg of nose-down twist. Rotor thrust was measured using a strain gauge balance, and rotor power was measured using a torque disk. The tail of the body was made sufficiently long to ensure that the rear boundary of the rotor wake impinged on the body

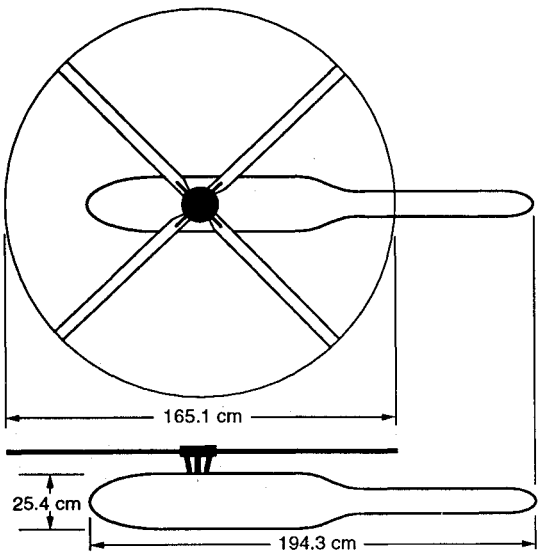

Fig. 1 Rotor/body system.

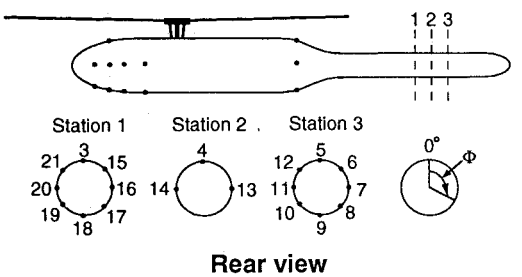

Fig. 2 Location of pressure transducers.

surface unimpeded by any other airframe components. Further details of rotor/body system are given in Ref. 21.

A total of 32 pressure sensors were located at key points on the body surface, as shown in Fig. 2. The sensors were mainly concentrated at three circumferential locations on the tail, which are identified as stations 1–3. The stations were spaced 5.2-cm (2-in.) apart. Based on results from previous experiments,[10] the tip vortices trailed from the rear of the rotor disk were known to approach and impinge the body surface near these locations at low advance ratios. At stations 1 and 3, eight pressure sensors were mounted with equiangle spacing around the circumference. At station 2, transducers were placed on the top centerline and on both sides.

The outputs from the sensors were connected to a multichannel, high-speed data acquisition system. The signals from each channel were amplified, and then sampled simultaneously by a bank of 12-bit A/D converters. Further details of the data acquisition system are given in Ref. 21. Time histories of all the sensor responses were logged over 10 rotor revolutions, with a sampling resolution of 1.4 deg of rotor azimuth (256/revolution). This was a sufficiently high sampling frequency to resolve all unsteady pressure fluctuations of interest. The data were filtered to remove fluctuations above 4 kHz.

The wide-field shadowgraph technique was used to visualize the rotor wake and the qualitative processes involved in the tip vortex interactions with the body. In essence, the apparatus consists of a high-intensity, short duration point source strobe light, a retroreflective screen, and a camera. Due to refraction effects in the flow, the shadowgraph method produces a projection of any rotor wake features with significant density gradients (such as the tip vortices) onto the flat screen. The extremities of this shadowgraph image essentially constitute a cross section of the wake boundary at the longitudinal centerline directly above the body surface. This technique was

found to be extremely useful in helping locate the trajectories of the tip vortices relative to the longitudinal centerline of the body. Test conditions such as advance ratio and rotor thrust varied in real-time to ensure that the tip vortex filaments comprising the rear wake boundary impinged on the body surface near the desired location. Further details of the wide-field shadowgraph technique, and the procedure used to quantify the vortex trajectories, can be found in Ref. 24.

Test Procedure

The experiments were performed in the University of Maryland's Glenn L. Martin wind tunnel. This is a closed-return wind tunnel with a 2.36 × 3.35 m (7.75 × 11 ft) working section. The rotor was tested at a rotational speed of 1980 rpm (33 Hz), which corresponded to a nominal tip Mach number of 0.5 in hover. The tests were conducted by turning the rotor at the required rotational speed, increasing the tunnel wind speed, while adjusting collective pitch and trimming the rotor to the desired test conditions. The trim procedure was performed by adjusting lateral and longitudinal cyclic pitch inputs by way of the swashplate to eliminate the once-per-revolution blade flapping response relative to the shaft. The flapping was measured using Hall-effect sensors at the flap hinges. This ensured that the rotor tip-path plane (TPP) was perpendicular to the rotor shaft axis, and therefore, also parallel to the longitudinal centerline of the body. The rotor coning angle was about 3 deg under all test conditions.

Tests were conducted at seven advance ratios, namely μ = 0.05, 0.06, 0.065, 0.07, 0.075, 0.08, and 0.1. At each advance ratio, results for two representative blade loading coefficients of C_T/σ = 0.075 and 0.09 were recorded. A single TPP angle of −6 deg (forward shaft tilt) was used, since it was found that unsteady pressures on the body surface were insensitive to TPP angle of attack.

Results and Discussion

Pressure Loads on the Body Surface

The unsteady pressure data presented in this article are event-averaged, i.e., the data were first ensemble-averaged over 10 rotor revolutions, and since a four-bladed rotor was used, the results were further ensemble-averaged over 90 deg of blade azimuth angle. For presentation, the time histories of the event-averaged data are shown over a full 360 deg of rotor azimuth. In addition, all the unsteady pressure data presented represent the fluctuations of the measured pressures about the mean value. The maximum likely estimated error in C_p^u was about ±0.10.

Representative Unsteady Pressures on the Body Surface

As discussed in Ref. 4, four characteristic pressure signatures on the body surface can be discerned during rotor/body testing. These signatures are due to 1) the effects of blade passage, 2) close tip vortex/surface interactions, 3) tip vortex/surface impingement, and 4) postvortex/surface impingement.

Figure 3a shows a typical unsteady pressure signature caused by blade passage effects. This type of loading is characterized by a N_b/revolution pressure pulsation, with the peak pressure occurring in phase with the blade passage over the body, i.e., at integer multiples of 90 deg. The unsteady loads induced by blade passage effects are essentially proportional to rotor thrust (blade lift or bound circulation), and are largely independent of the advance ratio, i.e., independent of the location of the blade tip vortices.[4] The feature of blade passage induced loads have been shown to be predictable by means of unsteady potential flow theory.[6]

Figure 3b shows a type of signature that has been previously classified as a close tip vortex/surface interaction. Close vortex/surface interactions occur when the rotor tip vortices pass close to the measurement point, but do not impinge on the body surface until some distance downstream. Figure 3c shows the pressure signature that results from tip vortex impingement on the body surface near the measurement point. It is characterized by a transient loading with high suction pressure and associated pressure gradient due to the proximity of the vortex core. Just downstream of the vortex impingement point, Fig. 3d shows that multiple pressure peaks are produced, which is probably indicative of boundary-layer separation and secondary vorticity creation near the body surface.

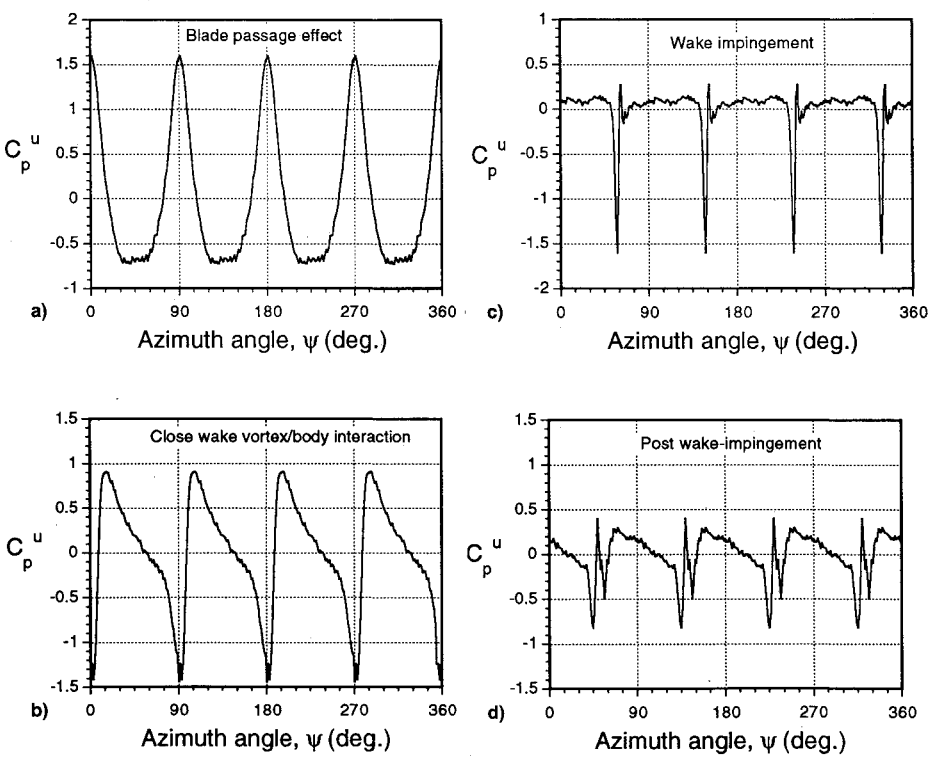

Fig. 3 Representative unsteady pressures on body.

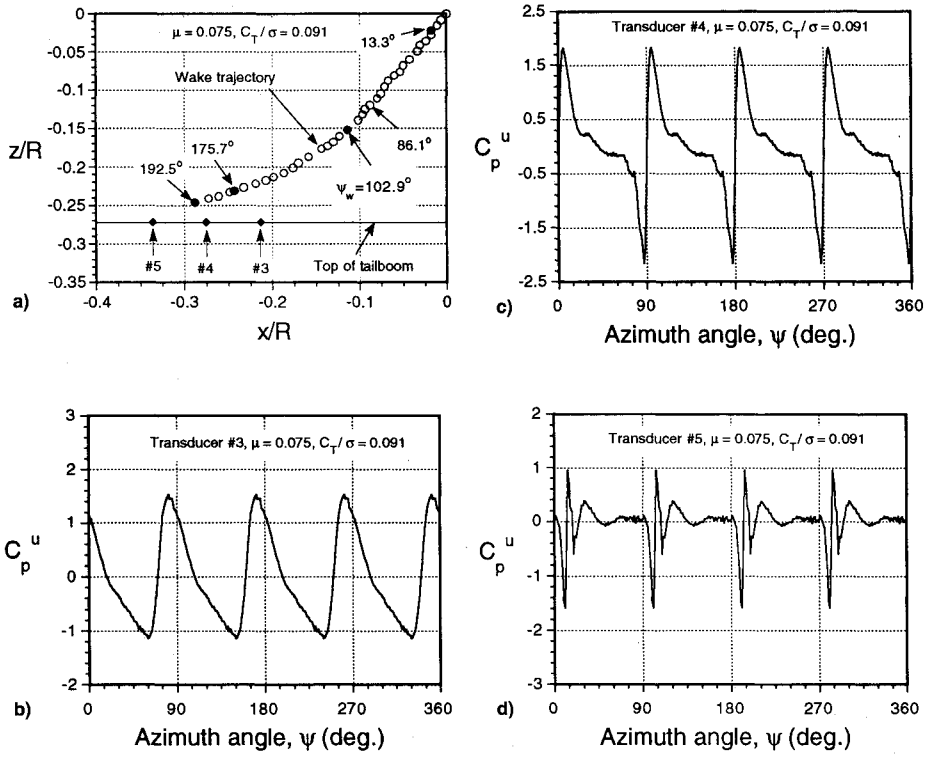

Fig. 4 Wake trajectory and associated unsteady pressures for $\mu = 0.075$.

Tip Vortex Trajectories and Pressure Signatures

The relationship between the tip vortex positions at the longitudinal centerline of the wake and the unsteady pressure responses induced on the body surface was investigated. The measurements were all made downstream of the rotor on the tail of the body to ensure that the pressure loads due to blade passage were negligibly small, and therefore, did not dominate the loads induced by the tip vortices, unlike the work of Ref. 3. It has been shown that blade passage effects diminish quickly away from the rotor disk,[6] therefore, the present measurements almost completely isolate the effects of the body on the tip vortices, and hence, the effects of the convecting tip vortices on the body loads.

Figure 4a shows the geometry of the rear wake boundary (or tip vortex trajectory) at the longitudinal centerline of the wake, as measured from the shadowgraphs, for an advance ratio of 0.075 at $C_T/\sigma = 0.091$. Figures 4b–4d show the corresponding unsteady pressures measured on the top centerline of the body at stations 1–3, i.e., at sensor locations nos. 3, 4, and 5, respectively. Note that the origin of the coordinate system used for the tip vortex trajectory is the reference blade tip location when it passes over the centerline of the tail, i.e., at a blade azimuth angle, $\psi = 0$ deg. The wake trajectories and transducer locations are all measured relative to this reference.

Figure 4a shows that as the blade tip vortices are convected downwards, the local skew angle of the wake boundary relative to the vertical becomes progressively larger near the body surface. This is mainly due to the image effects induced by the surface. Note that the wake trajectory approaches an asymptote that is almost parallel to the body surface. The distance between the asymptote and the top of tail was found to be approximately 10% of the body diameter for all the advance ratios tested. Since two-dimensional potential flow theory predicts that a convecting vortex will asymptotically approach a solid surface, the observed behavior suggests the development of a local three-dimensional induced velocity field, and possibly viscous effects close to the body surface.

Figure 4a also shows that the tip vortices pass above sensor location nos. 3 and 4 at $\mu = 0.075$, and closely approach the body surface just upstream of location no. 5. The pressure signature recorded at location no. 5 indicates postvortex/surface impingement, so that location nos. 3 and 4 must be located upstream of the vortex impingement point. The unsteady pressure measured at location no. 4 is representative of a close vortex/surface interaction, and this confirms the location of impingement downstream of this point, as shown in Fig. 4b. In Fig. 4a, the tip vortex positions with the wake ages marked correspond, approximately, to the pressure peaks occurring in Fig. 4c. At location no. 3, the pressure signature is similar in shape to that due to the blade passage effects (as shown in Fig. 4c), since the tip vortices are convected further above the transducer and more parallel to the body surface.

The tip vortex trajectory and induced pressure loads on the top surface centerline of the tail for a lower advance ratio of 0.065, and at the same nominal C_T/σ, are shown in Fig. 5. At this lower advance ratio, the vortex impingement point has now moved upstream from near location no. 5 to the vicinity of location no. 4, as shown in Fig. 5a. Therefore, only the pressure signature measured at location no. 3 represents a close vortex/surface interaction. The unsteady pressure measured at location no. 4 is clearly due to vortex impingement on the surface. The corresponding positions of the vortices that produced the negative pressure peaks shown in Fig. 5c are marked with their ages in Fig. 5a. Downstream of vortex impingement, the ensemble-averaged pressure responses were found to be fairly benign, suggesting significant diffusion or splitting of the tip vortices after the impingement.

Sensitivity of Unsteady Pressures to Changes in Advance Ratio

The above results show that the unsteady pressures measured upstream and downstream of the tip vortex impingement point, respectively, have very distinct characteristics. Clearly, slight changes in advance ratio may significantly change the wake position and vortex trajectories, and therefore, alter the pressure loads at a given point on the body. It is very difficult to calculate the tip vortex trajectories exactly, however, calculations based on classical momentum theory can be used to illustrate the general sensitivity of the wake boundary impingement location to changes in advance ratio.

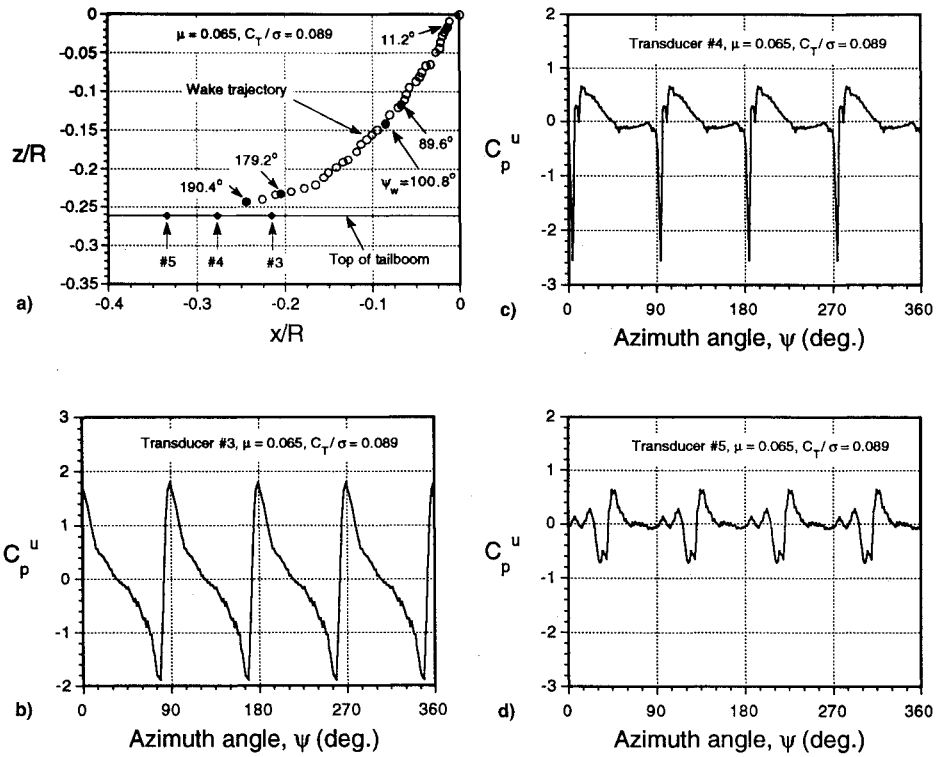

Fig. 5 Wake trajectory and associated unsteady pressures for $\mu = 0.065$.

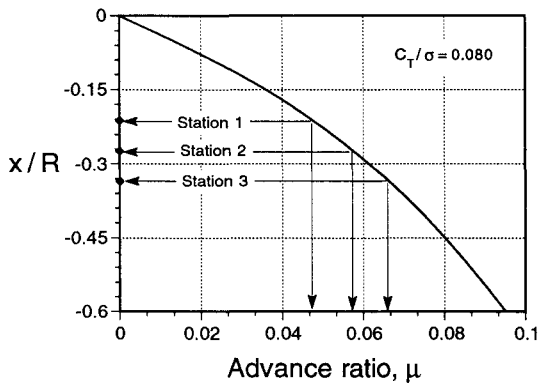

Fig. 6 Effects of advance ratio on the wake impingement location.

From momentum theory, the relationship between the mean skew angle of the wake boundary χ and the advance ratio μ can be expressed as

$$\chi = \tan^{-1}(\mu/\lambda) \tag{1}$$

where λ is the mean inflow ratio across the rotor disk. The inflow ratio is given by

$$\lambda = [C_T/(2\sqrt{\mu^2 + \lambda^2})] + \mu\alpha_{TPP} \tag{2}$$

which can be solved iteratively for λ. Figure 6 shows that at a constant thrust, small increments in advance ratio move the wake boundary, and therefore, the tip vortex impingement location, rather significantly. For example, although there is only a 3-deg difference in the wake skew angle when the advance ratio is changed from 0.07 to 0.075, the vortex impingement point on the body moves approximately 2.5-cm (1-in.) downstream, i.e., half the distance between successive body measurement stations.

The measured effects of small changes in advance ratio on the pressure responses on the top centerline of the body are shown in Fig. 7 for a single point (location no. 4). The results are plotted for changes in advance ratio in steps of 0.005, and at a constant $C_T/\sigma = 0.09$. The unsteady pressures for $\mu = 0.05$ are benign since location no. 4 was located downstream of the tip vortex impingement point. For $\mu = 0.06$, the large transients coupled with the secondary peaks in the pressure signature shown in Fig. 7b suggest that the tip vortices impinged on the body surface just upstream of location no. 4. The vortices induce these high-suction pressure peaks only when they are in close proximity to the measurement point. Furthermore, when the vortex is sufficiently near the surface, the adverse pressure gradient thus created, along with the pressure gradient caused by the mean downwash,[21] may be strong enough to cause local flow separation. The secondary peaks in the pressure signature shown in Fig. 7b are probably due to eruption of the surface boundary layer and the creation of secondary vorticity. Secondary vortex creation is a documented phenomenon when vortices approach solid boundaries at low Reynolds numbers,[14] yet these secondary structure(s) are obviously much weaker since no evidence of secondary vortex structures could be discerned here from the shadowgraph flow visualization.

As the advance ratio was further increased from 0.06 to 0.065, the measured pressure response shown in Fig. 7c indicated direct tip vortex impingement at location no. 4. The large transient suction pressures are evidence that the high peripheral velocities at the cores of the tip vortices were in proximity to the sensor location. By increasing the advance ratio further from 0.065 to 0.07, the unsteady pressure response at location no. 4 changed from that due to vortex/surface impingement to a close vortex/surface interaction, as shown by Fig. 7d. Since the wake boundary was more highly skewed at $\mu = 0.070$ than at $\mu = 0.065$, the vortex impingement point moved further downstream, such that transducer no. 4 was now located just upstream of vortex impingement. All the unsteady pressures measured at location no. 4 for advance ratios greater than 0.070 were representative of close vortex/surface interactions, as shown in Figs. 7e and 7f for advance ratios of 0.075 and 0.08, respectively.

The close vortex/surface interaction loads are clearly very sensitive to the proximity and velocity at which the core of the tip vortices pass over the body. Figures 7e and 7f show

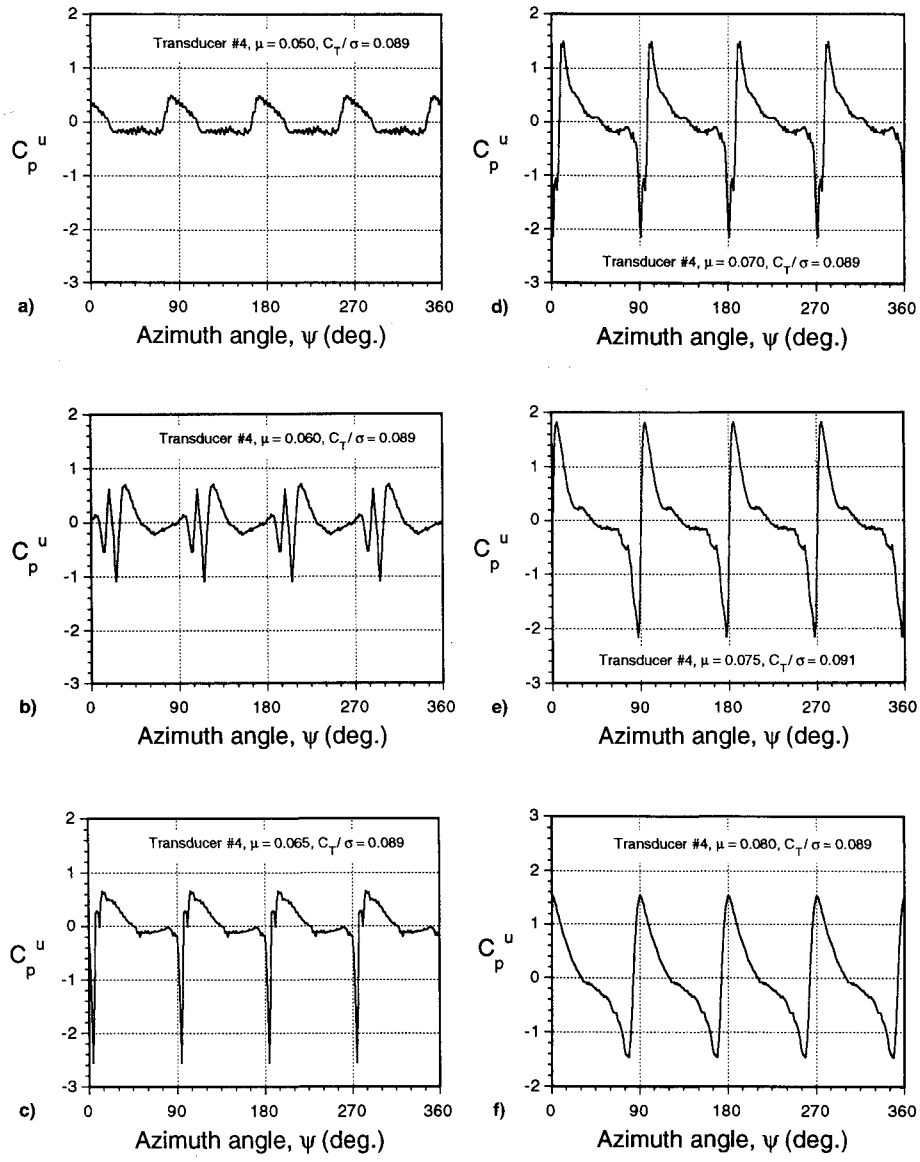

Fig. 7 Sensitivity of unsteady pressures to changes in advance ratio.

that though both pressure signatures represent close vortex/surface interactions, there are still some differences due to only a 0.005 change in advance ratio. First, the peak-to-peak value of the unsteady pressures is 4.0 at $\mu = 0.075$, while the peak-to-peak value at $\mu = 0.080$ drops only to 3.0, i.e., a 25% reduction in magnitude due to a 0.005 change in advance ratio. Second, there is about a 15-deg difference in phasing between the peaks of these two pressure signatures. This is because the tip vortices are convected through the flowfield slightly faster at $\mu = 0.080$ than at $\mu = 0.075$, therefore, the pressure peaks at the same point on the body surface occur at different times, i.e., at different wake ages or blade azimuth angles.

It is important to note that the unsteady pressure signatures measured on the body depend not only on the relative location of the rotor tip vortices, but also on the vortex strengths (i.e., the rotor thrust), and their convection velocity through the flow (i.e., advance ratio). Changes in rotor thrust will change both the strength of the rotor tip vortices as well as the mean downwash induced by the rotor. Therefore, changes in thrust at a constant advance ratio will relocate the rotor wake position [see Eqs. (1) and (2)]. While such effects were examined in the experiment, the overall results were found to be qualitatively similar to those obtained by changing advance ratio, and will not be discussed further.

Unsteady Pressures Around the Body Circumference

One interesting problem that is poorly understood, is the three-dimensional behavior of the tip vortices when close to the body surface. It is clear from the foregoing that the tip vortices undergo distortions close to the top of the body, and ultimately come close enough to the surface to produce adverse pressure gradients that cause an eruption of the boundary layer. Yet, it is not clear if, or to what extent, the blade tip vortices wrap around the body after they impinge the body surface, or as to the persistence of the tip vortex structure after the impingement. It is difficult to examine the vortex filaments on the sides of the body using any flow visualization technique, however, based on the previous discussion, it is possible to infer the locations of the vortices on the sides of the body directly from the unsteady pressure measurements.

Figure 8 shows the unsteady pressures measured around the circumference of the body at station 3 on the body (see Fig. 2) for an advance ratio of 0.08 and at $C_T/\sigma = 0.091$. This figure shows that the pressure signatures at a single body section vary dramatically, ranging from those representative of close vortex/surface interactions, to vortex/surface impingement, and postvortex/surface impingement. Figure 8b shows that vortex impingement occurs close to sensor location no. 6 ($\Phi = 45$ deg), i.e., on the right (advancing) side of the

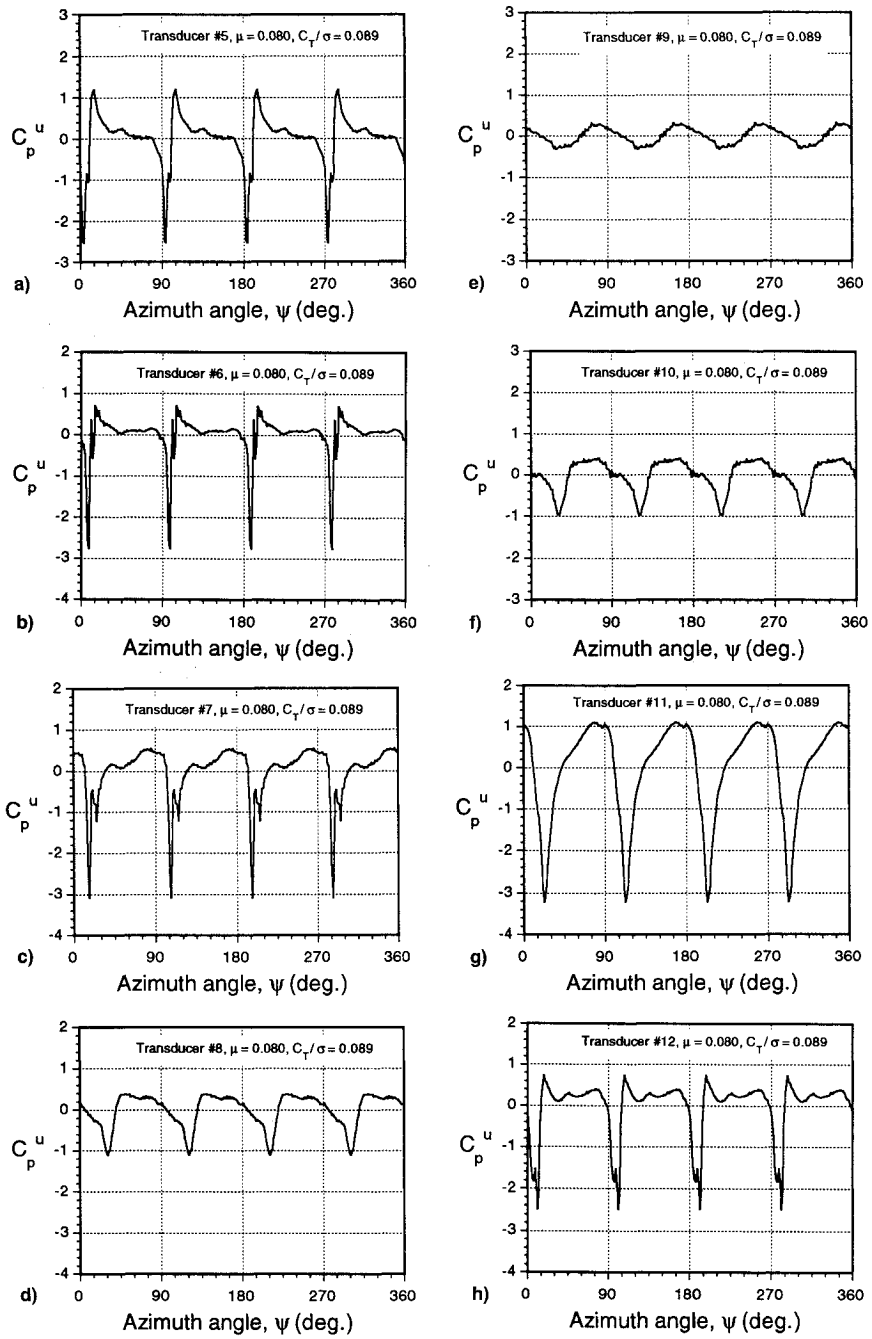

Fig. 8 Unsteady pressures measured around the body circumference.

body. On the top of the body (location no. 5) and on the retreating side at location nos. 12 and 11 (Figs. 8a, 8h, and 8g, respectively), pressure signatures characteristic of close vortex/surface interactions are produced. This suggests a lateral skewness of the wake, biased toward the advancing side of the rotor. It is a well-known result that the mean downwash velocity is higher on the advancing side of a rotor in forward flight. From a thorough examination of pressure measurements at other body stations and for different test conditions, it was found that the tip vortices always impinged first on the advancing side of the body. A three-dimensional interpretation of tip vortex impingement on the body is schematically shown in Fig. 9.

At location no. 7 (Φ = 90 deg), as shown by Fig. 8c, the unsteady pressure signature was indicative of postvortex/surface impingement, since the characteristic secondary pressure peaks were produced. This confirms that the vortices impinged on the advancing side of the body upstream of location no. 7. At locations no. 8 (Φ = 135 deg), no. 9 (Φ = 180 deg), and no. 10 (Φ = 225 deg), as shown in Figs. 8d–8f, respectively, the unsteady pressures suggest close vortex/surface interactions. These latter results show that the vortex filament was, at least partially, wrapped around the body surface during the impingement process.

From a further examination of other unsteady pressure measurements, no direct evidence of the tip vortex was found over the lower part of the body surface (in the region from Φ = 135 deg to Φ = 225 deg) under any test conditions, even at lower advance ratios. This suggests that the tip vortex is split, and vorticity is quickly diffused after the impingement. However, the unsteady pressure responses measured on the underside of the body were generally still significant, e.g., as shown in Fig. 8e. This suggests that other parts of the tip vortex, or some remnants of it, are still strong enough to produce measurable loads. Only faint and highly nonperiodic vortex filaments were observed underneath the body from the shadowgraphs.

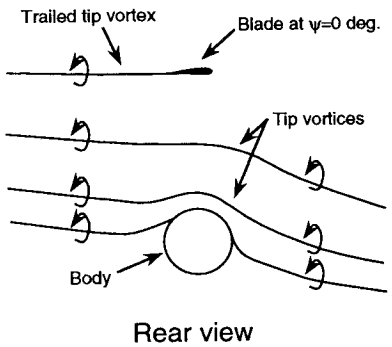

Fig. 9 Schematic of wake impingement on the body.

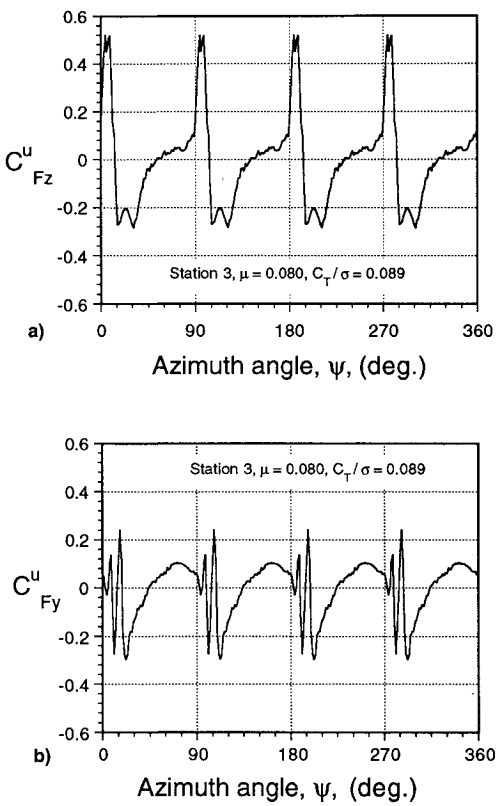

Fig. 10 Normal force and side force at station three on the tail.

Forces on Tail

As shown above, there are considerable differences between the pressures measured on the advancing, retreating, top, and bottom sides of the body. These differences can cause large unsteady forces on the body. To obtain these forces (approximately), the unsteady pressures around the stations on the tail were integrated numerically.

Figure 10a shows the time history of the normal force coefficient at station 3. It was found that the characteristics of the normal force were similar to those of the unsteady pressure signatures due to close vortex/surface interactions. This shows that the airloads induced by close vortex interactions are the main contributors to the unsteady normal force induced on the body section. The behavior of the unsteady side force coefficient is somewhat more complicated, as shown by Fig. 10b. Though the basic form of the loading shows that the close vortex/surface interaction process is still the main contributor to the side force, the multiple peaks responses indicate that the vortex impingement is a significant source of higher harmonics in the loading. These results perhaps emphasize the need to model the induced loads due to close vortex/surface interactions, as opposed to vortex impingement effects when the total loads on airframe are required.

Unsteady Potential Flow Theory

As demonstrated in the experiment, small changes in rotor tip vortex positions can make large differences in the magnitude and character of the pressure response at a given location on the body. This sensitivity makes the analytical prediction of the airloads difficult since the rotor tip vortex positions must be calculated with a high level of precision. No currently available rotor wake model has, of yet, demonstrated the required precision.

To help eliminate the uncertainty in predicting the rotor wake geometry, the tip vortex trajectories at the longitudinal centerline (as obtained from the flow visualization) were used to directly prescribe the locations of the vortices as functions of time. The calculated pressure responses on the surface were then compared with the measured pressures. By prescribing the vortex trajectories, an evaluation of the adequacy and limitations of potential flow theory for use in interactional aerodynamics can be made, without overconcern for uncertainties associated with the position and velocity of the tip vortices. From the shadowgraph results, it was possible to quantitatively measure the locations of the tip vortices at the longitudinal centerline of the rotor, that is in the longitudinal plane of the body.

Since the tip vortex filaments have a large radius of curvature (rotor radius/tail radius = 16.3) a two-dimensional model of the problem was used. This model consisted of a series of rectilinear vortices, representing the aft boundary of the rotor wake, approaching an infinite flat surface. The surface was made a streamline to the flow by the inclusion of image vortices below the surface. An exponential curve fit to the vortex displacements was chosen because of the asymptotic nature of the vortex trajectories close to the body surface. The x and z components of the vortex convection velocity at any instant were calculated analytically from these curve fits.

In unsteady flow, the pressure coefficient at a point on the body surface can be computed from

$$C_p^u = \left(V_\infty^2 - v^2 - 2\frac{\partial \phi}{\partial t}\right)\frac{100}{(\Omega R)^2} \tag{3}$$

which follows directly from the unsteady Bernoulli equation. The quasisteady velocity term is computed by means of the Biot-Savart law, whereas the unsteady potential term, $\partial\phi/\partial t$, accounts for the unsteady effects associated with the convecting vortices. It can be shown that for a two-dimensional flow with a single vortex, this unsteady term can be written as

$$\frac{\partial \phi}{\partial t} = -\boldsymbol{V}_i \cdot \boldsymbol{V}_{\text{vor}} \tag{4}$$

where $\boldsymbol{V}_i$ is the velocity induced at a point by the vortex, and $\boldsymbol{V}_{\text{vor}}$ is the convection velocity of the vortex. The net quasisteady and unsteady effect of all the vortices and their image system is finally obtained by superposition.

The strengths of the rotor tip vortices must also be determined, and can be related to the rotor thrust. For a rotor with uniform circulation in hover, the exact result is

$$\Gamma = kc\Omega R(C_T/\sigma) \tag{5}$$

where $k = 2$.[25] For the purposes of the present work, the circulation was calculated using the value $k = 2.4$, as given by Beddoes.[26] This approximately accounts for the nonuniform blade circulation and tip loss effects.

Comparison Between Theory and Experiment

Two advance ratios were considered for comparison with the theory, namely $\mu = 0.065$ and 0.075. Both cases were for

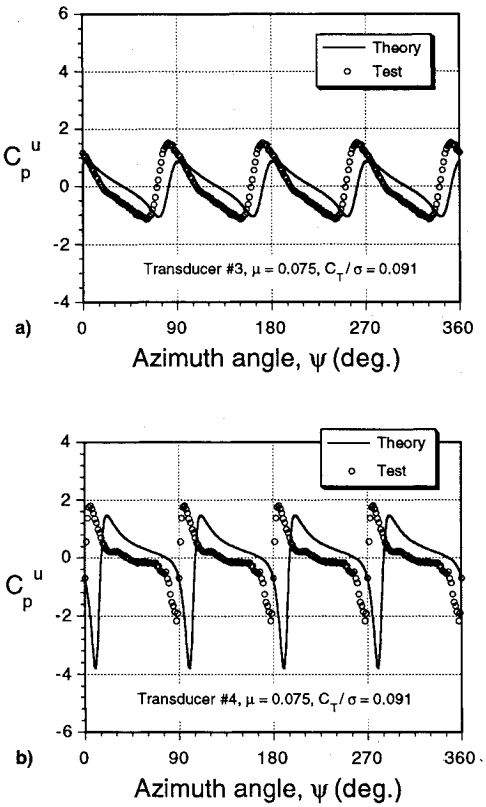

Fig. 11 Unsteady pressure predictions on the body at $\mu = 0.075$.

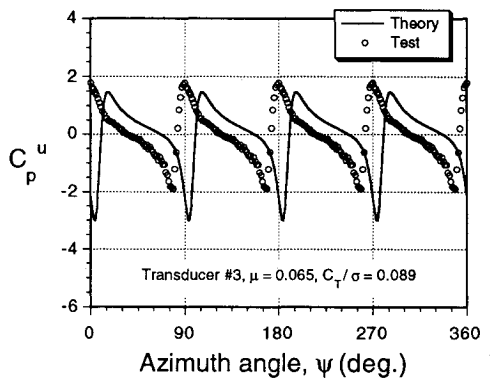

Fig. 12 Unsteady pressure predictions on the body at $\mu = 0.065$.

a nominal blade loading of $C_T/\sigma = 0.09$. Figure 11 presents comparisons of the theory with test data for an advance ratio of $\mu = 0.075$ at two different sensor locations, nos. 3 and 4. As shown previously in Fig. 4, the tip vortices impinge on the body downstream of location no. 4 at this advance ratio. The pressure signature measured at location no. 3 is dominated by the unsteady ($\partial\phi/\partial t$) contribution, since the tip vortices are higher above the body surface at this station and the quasi-steady term is small. As the tip vortices approach the body more closely (impingement occurs downstream at location no. 4), the quasisteady contribution becomes more significant, and the net pressure response suggests a close vortex/surface interaction. The two-dimensional model predicts the pressure signatures fairly well, but even though the tip vortex velocity and spatial locations were prescribed, phase differences are still evident in both comparisons. For the lower advance ratio of 0.065, the tip vortices impinge on the surface near transducer no. 4. Thus, the pressure induced at no. 3 represents a close vortex/surface type of interaction. Again, except for the phase shift, the calculated pressure signature is in good agreement with the experimental measurements shown in Fig. 12, suggesting that three-dimensional effects are small.

Theoretically, there is a one-to-one relationship at any time between the vortex location(s) and the pressure response. The azimuthal time when pressure peaks occur can be selected as checkpoints, since at these times a vortex will be near the measurement point. Figure 11b shows that the pressure signature measured at location no. 4 has a negative suction peak at $\psi = 174$ deg and a positive peak at $\psi = 186$ deg. Both positive and negative pressure peaks will occur a short time after a vortex passes over the measurement point, therefore, the theory predicts that the vortex should be about 170-deg old when it passes over location no. 4. However, from the unsteady pressure predictions made using the measured tip vortex trajectories, it shows that the vortex age is about 190 deg when passing over location no. 4. The reason for this difference is partly the difficulty in measuring the tip vortex trajectories to the required level of precision. Also, the two-dimensional nature of the model itself must be questioned when the tip vortex comes very close to the body surface and three-dimensional distortion begins to occur. However, the overall agreement with the test data is encouraging, and for practical calculations of total and sectional body loads, the results lend support to the use of potential flow models of the problem.

Conclusions

Wind-tunnel tests were conducted to investigate the unsteady aerodynamic interactions between rotor tip vortices and a body in low-speed forward flight. The wide-field shadowgraph method was used to visualize the rotor tip vortices during the interactions. The pressure signatures measured on the top of the tail were correlated with the observed tip vortex trajectories. Unsteady potential flow theory was also explored for predicting the unsteady pressure loads on the top of the body using measured vortex trajectories.

The following conclusions have been drawn from present study:

1) The measurements have confirmed that the pressure signatures at specific points on the body showed very distinct characteristics which were sensitive to the proximity and trajectories of the vortices. The unsteady pressures at a given point were found to be particularly sensitive to changes in the advance ratio at a constant rotor thrust.

2) Tip vortex impingement induces large transient loads on the body surface, coupled with a high adverse pressure gradient and possible eruption of the boundary layer. However, vortex impingement is a very localized problem on the airframe, and may not contribute significantly to the total body airloads. In practice, tip vortex impingement will only occur on helicopters operating in hover or at low advance ratios.

3) The features of the pressure signatures measured around the circumference of the body were particularly complicated, ranging from close vortex/surface interactions to vortex/surface impingement. It was deduced that the tip vortices were skewed laterally as well as longitudinally as they approached the body surface. The vortex filaments always impinged on the side of the body on the advancing side of the rotor.

4) It was shown that some aspects of the vortex/surface interaction problem can be successfully modeled using a two-dimensional potential flow analysis. However, when the vortices closely approach the surface, three-dimensional effects and viscous interactions appear important. Fortunately, the region in which this is important on helicopters is somewhat small, and an inviscid analysis using conventional mathematical models of the rotor wake may be useful over the majority of the body surface.

Acknowledgments

This work was supported by the U.S. Army Research Office under Contract DAAL-03-88-C002. Additional support for the shadowgraph studies was provided by the Rotorcraft Aeromechanics Branch at NASA Ames under Grant NAG2-

607. The authors thank Rotorcraft Center research engineer Dhananjay Samak for his assistance in conducting the experiments, Ashish Bagai for helping with the shadowgraph results, and Jewel Barlow for his cooperation in accommodating the tests in the Glenn L. Martin wind tunnel. The authors also thank the reviewers of this article for their insightful comments and helpful suggestions.

References

[1]Bramwell, A. R. S., "A Theory of the Aerodynamic Interference Between a Helicopter Rotor Blade and a Fuselage and Wing in Hovering and Forward Flight," *Journal of Sound and Vibration*, Vol. 3, No. 3, 1966, pp. 355–383.

[2]Sheridan, P. F., and Smith, R. P., "Interactional Aerodynamics—A New Challenge to Helicopter Technology," 35th Annual Forum of the American Helicopter Society, Washington, DC, May 1979.

[3]Komerath, N. M., McMahon, H. M., Brand, A., Liou, S. G., and Mavris, D., "Prediction and Measurement of the Aerodynamic Interactions Between a Rotor and Airframe in Forward Flight," *Proceedings of the 45th Annual Forum of the American Helicopter Society*, Boston, MA, May 21–24, 1989.

[4]Bi, N.-P., and Leishman, J. G., "Analysis of Unsteady Pressures Induced on a Body in the Vicinity of a Rotor," *Journal of Aircraft*, Vol. 28, No. 11, 1991, pp. 756–767.

[5]Prouty, R. W., "Importance of Aerodynamics on Handling Qualities," *Proceedings of the American Helicopter Society National Specialists' Meeting on Aerodynamics and Aeroacoustics*, Arlington, TX, Feb. 1987.

[6]Crouse, G. L., Leishman, J. G., and Bi, N.-P., "Theoretical and Experimental Study of Unsteady Rotor/Body Aerodynamic Interactions," *Journal of the American Helicopter Society*, Vol. 37, No. 1, 1992, pp. 55–65.

[7]Quackenbush, T. R., Bliss, D. B., Lam, C.-M. G., and Katz, A., "Free Wake Calculation of Rotor Flow Fields for International Aerodynamics," *Proceedings of the 46th Annual Forum of the American Helicopter Society*, Washington, DC, May 21–23, 1990.

[8]Fradenbergh, E. A., "Aerodynamic Factors Affecting Overall Hover Performance," *AGARD Conference Proceedings No. 111*, Paper 6, Feb. 1973.

[9]Bagai, A., and Leishman, J. G., "A Study of Rotor Wake Development and Wake/Body Interactions in Hover," *Proceedings of the Third International Specialists' Meeting on Rotorcraft Basic Research*, Georgia Inst. of Technology, Atlanta, GA, March 25–27, 1991.

[10]Leishman, J. G., and Bi, N.-P., "Measurements of a Rotor Flowfield and the Effects on a Body in Forward Flight," *Vertica*, Vol. 14, No. 3, 1990, pp. 401–415.

[11]Lim, T. T., "An Experimental Study of a Vortex Ring Interacting with an Inclined Wall," *Experiments in Fluids*, Vol. 7, No. 7, 1989, pp. 453–463.

[12]Atias, M., and Weihs, D., "Motion of Aircraft Trailing Vortices Near the Ground," *Journal of Aircraft*, Vol. 21, No. 10, 1984, pp. 783–786.

[13]Doligalski, T. L., and Walker, J. D. A., "The Boundary Layer Induced by a Convected Two-Dimensional Vortex," *Journal of Fluid Mechanics*, Vol. 139, Feb. 1984, pp. 1–28.

[14]Walker, J. D. A., Smith, C. R., Cerra, A. W., and Doligalski, T. L., "The Impact of a Vortex Ring on a Wall," *Journal of Fluid Mechanics*, Vol. 181, Aug. 1987, pp. 99–140.

[15]Brand, A. G., Komerath, N. M., and McMahon, H. M., "Results from a Laser Sheet Visualization of a Periodic Rotor Wake," 26th Aerospace Science Meeting, AIAA Paper 88-0192, Reno, NV, Jan. 11–14, 1988.

[16]Leishmann, J. G., and Bagai, A., "Shadowgraphic Flow Visualization of a Rotor Wake in Low Speed Forward Flight," VHS Video, Dept. of Aerospace Engineering, Univ. of Maryland, College Park, MD, Jan. 1991.

[17]Lorber, P. F., and Egolf, T. A., "An Unsteady Helicopter Rotor-Fuselage Interaction Analysis," NASA CR-4178, Aug. 1988.

[18]Komerath, N. M., McMahon, H. M., and Hubbard, J. E., "Aerodynamic Interactions Between a Rotor and Airframe in Forward Flight," AIAA 18th Fluid Dynamics and Plasmadynamics and Lasers Conf., AIAA Paper 85-1606, Cincinnati, OH, July 16–18, 1985.

[19]Brand, A. G., McMahon, H. M., and Komerath, N. M., "Surface Pressure Measurements on a Body Subject to Vortex-Wake Interaction," *AIAA Journal*, Vol. 27, No. 5, 1989, pp. 569–574.

[20]Crouse, G. L., and Leishman, J. G., "Interactional Aerodynamic Effects on Rotor Performance in Hover and Forward Flight," *Proceedings of the 48th Annual Forum of the American Helicopter Society*, Washington, DC, June 3–5, 1992, pp. 513–523.

[21]Leishman, J. G., and Bi, N.-P., "Aerodynamic Interactions Between a Rotor and a Fuselage in Forward Flight," *Journal of the American Helicopter Society*, Vol. 35, No. 3, 1990, pp. 22–31.

[22]Bi, N.-P., and Leishman, J. G., "Experimental Study of Aerodynamic Interactions Between a Rotor and a Fuselage," *Journal of Aircraft*, Vol. 27, No. 9, 1990, pp. 779–788.

[23]Clark, D., and Maskew, B., "A Re-Examination of the Aerodynamics of Hovering Rotors Including the Presence of the Fuselage," Third International Technical Specialists' Meeting on Rotorcraft Basic Research, Atlanta, GA, March 25–27, 1991; also at the 47th National Forum of the American Helicopter Society, Phoenix AZ, May 7–9, 1991.

[24]Leishman, J. G., and Bagai, A., "Fundamental Studies of Rotor Wakes in Low Speed Forward Flight Using Wide-Field Shadowgraphy," AIAA 9th Applied Aerodynamics Conference, AIAA Paper 91-3232, Baltimore, MD, Sept. 23–26, 1991.

[25]Stepniewski, W. Z., and Keys, C. N., *Rotary-Wing Aerodynamics*, Dover, New York, 1984.

[26]Beddoes, T. S., "A Wake Model for High Resolution Airloads," *Proceedings of the National Specialists' Meeting on Aerodynamics and Aeroacoustics*, Arlington, TX, Feb. 25–27, 1987.